Institut für Geophysik, Astrophysik und Meteorologie
Karl - Franzens - Universität Graz
Universitätsplatz 5, A-8010 Graz, Austria
http://www.uni-graz.at/igam

Wissenschaftlicher Bericht No. 15

# An efficient channel selection method for Infrared Atmospheric Sounding Interferometer data and characteristics of retrieved temperature profiles

by
E. Weisz, G. Kirchengast, and J. A. Lerner

March 2003

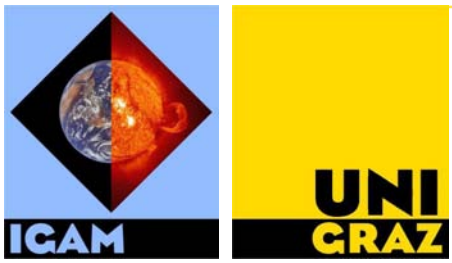

# An efficient channel selection method for Infrared Atmospheric Sounding Interferometer data and characteristics of retrieved temperature profiles

**E. Weisz [1], G. Kirchengast, and J. A. Lerner [2]**

Institute for Geophysics, Astrophysics, and Meteorology (IGAM), University of Graz, Universitätsplatz 5, A-8010 Graz, Austria

[1] Now at Space Science and Engineering Center, University of Wisconsin-Madison, 1225 W. Dayton Street, Madison, WI 53706, U.S.A.

[2] Now at Fleet Numerical Meteorology & Oceanography Center, Naval Research Lab, 7 Grace Hopper Ave, Monterey, CA 93943, U.S.A.

*Correspondence to:* G. Kirchengast

*E-Mail:* gottfried.kirchengast@uni-graz.at

[Author's Note: This report publishes a revised manuscript to *Annales Geophysicae*, February 2003. It is published in the *IGAM Wiss Ber.* series since the revised manuscript was still not endorsed by a reviewer (and based on this not accepted by the editor), who was skeptical that down-selection to ~1% of the IASI channels could lead to the retrieval performance shown. Given that the results were re-checked during revision very carefully and found o.k., and given the positive review of other peers providing encouragement to publish quickly, the skeptical review was considered not really fair and it was decided to have a fast publication this way.]

(intentionally left blank; back page if double-sided print)

**Abstract.** The Infrared Atmospheric Sounding Interferometer (IASI) is part of the core payload of the forthcoming series of European polar-orbiting operational meteorological satellites (METOP series; 1st launch scheduled 2005). Compared to existing operational satellite radiometers, the high spectral resolution IASI sensor (> 8000 channels from 3.6–15.5 μm) will allow, among other advances, improved accuracy and vertical resolution of retrieved temperature and humidity profiles. Exploiting this potential in applications like numerical weather prediction and climate change analysis requires advanced algorithms, which process the huge amount of spectral data in a fast and reliable way. We introduce an efficient and robust channel selection method, which retains at each retrieval level a small number of channels only, with the highest ratios of weighting function magnitude to radiometric error ("maximum sensitivity" channels). By one-to-one comparison of this "maximum sensitivity" method with a more elaborate selection method we found that the number of channels can be reduced based on this simple information content measure to as low as ~1% of the total number of channels (< 100 channels) without significantly degrading the quality of retrieved temperature profiles (i.e., retrieval error magnitudes change by ~10% or less only). Furthermore, utilizing the capabilities of the optimal estimation methodology employed in the retrieval processing, the effects of measurement noise and *a priori* uncertainties on retrieval performance are discussed as well as characteristic properties of the retrieved temperature profiles including correlation functions, weighting functions, resolution kernels, gain functions, and signal-to-noise functions. In general, IASI-derived temperature profiles exhibit an accuracy of ~1 K, at a resolution of 1 to 3 km, in the troposphere (below ~200 hPa). The theoretical error analysis and characterization was complemented by an ensemble-based empirical error analysis, which particularly addressed the impact of an (in)adequate choice of *a priori* profiles and their uncertainties. It is instructively shown that, for retrieving profiles with optimally minimized errors, any ensemble of *a priori* states should be statistically unbiased against the corresponding ensemble of "true" states as well as be consistent with the specified *a priori* error covariance matrix (in line with the assumptions of the optimal estimation framework used). The results of the study confirm the potential of IASI to significantly improve upon atmospheric information available from current meteorological satellite sounders.

(intentionally left blank; back page if double-sided print)

# 1 Introduction

The Infrared Atmospheric Sounding Interferometer (IASI) (e.g., Camy-Peyret and Eyre, 1998; Weisz, 2001; weblink http://smsc.cnes.fr/IASI/) is a novel high-resolution spectrometer of Fourier-Transform-Spectrometer (FTS) type for spaceborne sounding. Its radiometric measurements are based on Michelson interferometry covering the thermal infrared range from 645 $cm^{-1}$ (~15.5 μm) to 2760 $cm^{-1}$ (~3.6 μm) with a sampling interval of 0.25 $cm^{-1}$ (raw spectral resolution ~0.3–0.5 $cm^{-1}$), yielding 8461 channels in total. The instrument, while moving forward with the satellite platform, scans across track with a swath width of approximately ±1100 km. The instantaneous field of view (IFOV) is ~48 × 48 km at nadir, comprising 2 x 2 IASI detector pixels, each with ~12 km diameter. The total scan period is 8 seconds and consists of 30 IFOVs visited by the sensor in a so-called “step and dwell” mode.

One main objective of the IASI sensor, according to the “IASI Science Plan” (Camy-Peyret and Eyre, 1998), is to improve the accuracy and vertical resolution of temperature profiles available from spaceborne sounders to 1 K and 1 km, respectively, in the mid- to lower troposphere. This level of performance enables, for example, improvements in numerical weather prediction and more accurate monitoring of long-term changes in the thermal structure of the atmosphere. A more detailed introductory discussion of the potential scientific and operational utility of IASI was provided in Lerner et al. (2002), an initial investigation of the data quality to be expected for IASI temperature and humidity profiles.

In this study we focus on advancing the IASI data processing in the channel selection part for more efficient temperature retrievals and on performing a careful error analysis and characterization for retrieved temperature profiles. After introducing the forward model setup, a pre-requisite in the retrieval algorithm, in Section 2, we describe the channel selection procedures used in Section 3, in particular the new “maximum sensitivity” method. The optimal estimation retrieval algorithm and the various matrices required to characterize retrieval performance are introduced in Section 4. Results are presented and discussed in Section 5, including on channel selection, retrieval performance properties, and impact of (in)adequate modeling of *a priori* profiles and their uncertainties. Finally, a summary and main conclusions of the study are provided in Section 6.

## 2 Forward modeling

Proper modeling of the radiative transfer physics underlying an IASI brightness temperature measurement is essential for a successful retrieval of atmospheric temperature or humidity. We adopt here the optimal estimation methodology, an instructive and detailed description of which has been given recently by Rodgers (2000). Within this methodology, a forward model **f** describes how the measurements **y** are connected to the state vector **x**,

$$\mathbf{y} = \mathbf{f}(\mathbf{x}) + \boldsymbol{\varepsilon}, \qquad (1)$$

where $\boldsymbol{\varepsilon}$ is the measurement error including biases and random (instrumental) noise. The unbiased stochastic component of $\boldsymbol{\varepsilon}$ is statistically characterized by a measurement error covariance matrix $\mathbf{S}_\varepsilon$, including both instrumental/pre-processing errors (errors in **y**) and forward modeling errors (errors in **f**).

In the present context, **y** = **f**(**x**) denotes the infrared radiative transfer equation (e.g., Hanel et al., 1992), where **x** is the atmospheric state (essentially temperature, humidity and ozone profiles within a given IFOV of the sensor), **f**(**.**) is the mathematical expression of radiative transfer physics mapping **x** to **y**, and **y** assembles the brightness temperatures (or upwelling radiances) measured by the channels of the IASI sensor. As the equation of interest is moderately nonlinear, Eq. (1) is approximated by a Taylor expansion to 1st order,

$$\mathbf{y} = \mathbf{f}(\mathbf{x}_0) + \frac{\partial \mathbf{f}(\mathbf{x})}{\partial \mathbf{x}}(\mathbf{x} - \mathbf{x}_0) + \boldsymbol{\varepsilon}, \qquad (2)$$

with a suitable reference state vector $\mathbf{x}_0$. The derivative of the forward model **f** with respect to **x**, $\partial \mathbf{f}(\mathbf{x})/\partial \mathbf{x}$, is understood to be evaluated at $\mathbf{x} = \mathbf{x}_0$ and is termed weighting matrix (or Jacobian), hereafter denoted by $\mathbf{K}_0$ (or just **K**). The rows of **K**, each related to a specific element of **y**, are termed weighting functions.

The fast radiative transfer model RTIASI (Matricardi and Saunders, 1999) is used in order to simulate IASI measurements (i.e., brightness temperatures $\mathbf{T}_B$) and to compute the Jacobian with respect to temperature **T**, $\partial \mathbf{T}_B/\partial \mathbf{T}$. Briefly, the RTIASI model utilizes a 43 pressure level grid (or < 43 levels, dependent on the surface height chosen) from 0.1 mbar (~65 km height) to the surface. Accurate line-by-line transmittances (convolved with the IASI instrument spectral response function) and profile dependent

predictors are utilized to compute regression coefficients (fast transmittance coefficients) for a set of atmospheric profiles. These coefficients are needed to calculate transmittances (or optical depths) for any desired atmospheric input. By solving the radiative transfer equation, given temperature, humidity, and ozone profiles as input, the brightness temperatures $\mathbf{T}_B$ seen by the IASI sensor channels (or a selected subset of channels) as well as the Jacobian **K** are finally computed.

In order to realistically account for measurement noise, apodized random noise $\boldsymbol{\varepsilon}$ (dependent on $\mathbf{T}_B$ and wavenumber $\nu$, and including inter-channel correlation) is added to the simulated measurements $\mathbf{T}_B$, computed based on the best available current noise model for IASI brightness temperature data (P. Schluessel, EUMETSAT, Darmstadt, Germany, priv. communications, 2000; see Sect. 4 for more details).

## 3 Channel selection

Since a full IASI spectrum contains 8461 channels, it seems essential to reduce this number and to sensibly remove redundant information for purposes of computational efficiency and robustness of the retrieval algorithm. In practical terms, measurement information from a given ensemble of channels can be considered redundant if removing that ensemble from the complete measurement vector $\mathbf{T}_B$ produces an insignificant decrease in retrieval accuracy or resolution (e.g., fractional change of retrieval error or resolution < 10%).

A description of the basic steps of our channel reduction procedure has been given by Lerner et al. (2002); we briefly recall essentials here as to have sufficient context for introducing the new “maximum sensitivity” method. As a first step, channels with wavenumbers > 2500 $cm^{-1}$ (wavelengths < 4 μm) are removed as these are mostly surface channels or channels with methane sensitivity, which are not missed for temperature and humidity profiling. Moreover, dropping channels at wavelength < 4 μm also avoids potential problems with contamination by residual shortwave (solar) radiation not taken into account in the RTIASI model. Next, channels are removed with significant emission contributions from variable trace gas species other than the ones best aiding temperature and humidity retrieval ($CO_2$, $H_2O$, partially $N_2O$). While in this study $CO_2$ and $N_2O$ are treated as fixed gases in the RTIASI model, retrievals from real data should account for their variations (seasonal and trends), in particular in climatological studies. The “foreign” trace gases not of interest here include ozone ($O_3$),

methane ($CH_4$), carbon monoxide (CO), and cloroflourocarbons (CFCs). Also most of the "atmospheric window" region is dropped as not a high number of such channels is required for the intended upper air profiling. Carefully accounting for the "foreign" spectral features, the removed spectral bands include 825–1100 $cm^{-1}$ (9.1–12.1 μm; "atmospheric window", $O_3$, CFCs), 1220–1370 $cm^{-1}$ (7.3–8.2 μm; $CH_4$), and 2085–2220 $cm^{-1}$ (4.5–4.8 μm; CO, $O_3$), respectively. Figure 1 indicates these excluded spectral bands.

As there are still > 5000 channels available at this point, further reduction is warranted. We found it sensible to proceed now with a selection approach governed by two ingredients: 1) an information content measure quantifying the information a given channel will supply to the retrieval at a given pressure level and 2) a formulation for a target number of channels per retrieval level that does not yet degrade retrieval accuracy.

Lerner et al. (2002) implemented this generic approach by utilizing an elaborate information content measure introduced by Rodgers (1996) together with a heuristic formula for the target number of channels per level dependent on a few tuning parameters, which were fixed based on extensive retrieval performance tests. While this elaborate method led to quite reasonable results as reported by Lerner et al. (2002), it is desirable, in view of later large-scale applicability, to implement a simpler and more efficient method. Recent results by Rabier et al. (2001), who compared different channel selection methods, confirmed the high utility of the above approach but also pointed to the need for efficiency improvements to enable routine large-scale use of IASI data, such as assimilation into operational numerical weather prediction systems.

Below the Lerner et al. (2002) method (Sect. 3.1) is used as a reference for assessing the utility of the new "maximum sensitivity" method (Sect. 3.2). The assessment is done by one-to-one comparison of retrieval results from both methods (Sect. 5.1).

### 3.1 Information content theory

As used by Lerner et al. (2002) following Rodgers (1996), the information content (IC) can be viewed as the information gained by including a measurement or, alternatively, as a corresponding incremental reduction of uncertainty. It is a scalar measure, $H$, which was exploited by Lerner et al. (2002) at each retrieval level separately, considering only the channels peaking with their weighting function (row of $\mathbf{K}$) at that level, while Rodgers (1996) applied it globally to all channels together. $H$ reads

$$H = \tfrac{1}{2}\log_2\left|\mathbf{S}_a\hat{\mathbf{S}}^{-1}\right|, \quad (3)$$

with

$$\hat{\mathbf{S}} = [\mathbf{S}_a^{-1} + \mathbf{K}^T\mathbf{S}_\varepsilon^{-1}\mathbf{K}]^{-1}, \quad (4)$$

where $\hat{\mathbf{S}}$ is the retrieval error covariance matrix, $\mathbf{S}_a$ is the *a priori* error covariance matrix, $\mathbf{S}_\varepsilon$ is the measurement error covariance matrix, and $\mathbf{K}$ $(=\partial\mathbf{T}_B/\partial\mathbf{T})$ is the weighting matrix introduced in Sect. 2. The specification of $\mathbf{S}_a$ and $\mathbf{S}_\varepsilon$ is detailed in Sect. 4 below. Equations (3) and (4) are exploited in an iterative procedure, where always the channel with the highest $H$ is retained and removed from subsequent calculations. Before starting the iterative procedure, $\mathbf{K}$ is scaled with the aid of $\mathbf{S}_a$ and $\mathbf{S}_\varepsilon$, whereby the latter matrix is assumed diagonal. During the iterations $\mathbf{S}_a$ for the current step is taken to be $\hat{\mathbf{S}}$ from the previous step. The selection stops at a given level after a prescribed target number of channels has been retained. For a detailed description of the procedure see Rodgers (1996), Lerner et al. (2002), and Weisz (2001).

Figure 1a and 1b illustrate channel selection results based on this IC method for two different specifications of the target number of channels. The U.S. standard mid-latitude summer profiles were used to prescribe a typical atmospheric state. As vertical grid the 43 level grid of the RTIASI model was used, which is subsequently also used as retrieval grid. In the case of Fig. 1a we directly adopted the target number formulation of Lerner et al. (2002) and enabled selection of up to 10 % of the total number of channels peaking per level. A total of 866 channels was selected this way. In contrast, in the case of Fig. 1b we strongly restricted the allowed number of channels to 2 of those peaking per level, which led to a total of only 72 channels (less than 2 x 43 channels, since at a few levels no weighting functions are peaking, especially at and close to the surface; see Lerner et al., 2002).

### 3.2 Maximum sensitivity approach

Considering simplifications to the IC measure expressed by Eqs. (3) and (4), the most required features seem to be that instrument noise of selected channels should be small while at the same time their sensitivity to temperature (and humidity) perturbations, i.e., the weighting function values, should be high. The account for *a priori* information in

the IC measure seems less crucial (and might even be disadvantageous if only crude *a priori* information is available; see Sect. 5.3).

A matrix assembling ratios of weighting function values to measurement errors for all channels at all levels is an information content proxy neatly reflecting these considerations. More formally, we define a matrix **H** of the form

$$\mathbf{H} = \mathbf{S}_{\varepsilon,diag}^{-\frac{1}{2}} \mathbf{K} , \qquad (5)$$

where **K** and the diagonal measurement error covariance matrix $\mathbf{S}_{\varepsilon,diag}$ are contained (the off-diagonal elements of $\mathbf{S}_{\varepsilon}$ are disregarded in this context). According to Eq. (5), the parameters multiplied with the weighting matrix **K** are just inverse standard deviations (inverse square roots of the diagonal elements of $\mathbf{S}_{\varepsilon}$). In other words, matrix **H** assembles for each specific channel a weighting function scaled by the standard measurement error of that channel, i.e., its elements $H_{ij}$ express sensitivity-to-error ratios, which can well function as simplified scalar IC measures.

The selection procedure exploiting **H**, which we term "maximum sensitivity" (MS) method, is straightforward: Compute **H** by a single matrix multiplication (Eq. 5), which is very fast. Then, from top to bottom, select at each retrieval level *i* a prescribed target number $N_j$ of channels *j* with highest values $H_{ij}$ ("maximum sensitivity" channels) and retain them from subsequent selections at further levels. This selection process is very efficient as it is a simple column-by-column search of a predetermined number of maximum values (with masking out rows already selected).

Experimentation with many slightly more sophisticated variants of this simple MS method (first searching weighting function peaks as in the Lerner et al. (2002) method, more sophisticated search than just from top to bottom, etc.) indicated that none of these variants was able to provide an appreciable increase in retrieval performance. Thus all results shown for the MS method are directly based on the simple procedure described.

A somewhat akin (though less simple) selection method was recently also discussed by Rabier et al. (2001) under the term "Jacobian method", where channel selection was based on the signal-to-noise ratio matrix $\mathbf{H} = \mathbf{S}_{\varepsilon}^{-\frac{1}{2}} \mathbf{K} \mathbf{S}_{a}^{\frac{1}{2}}$ (cf. Eq. 10).

Figures 1c and 1d illustrate the channel selection results based on the MS method for two different target number specifications, 20 channels per level (Fig. 1c) or 2 channels per level (Fig. 1d), respectively. The former case led to 860 channels, while the latter yielded only 86 (2 x 43) channels.

After a number of channels has been selected either via the elaborated IC method or the simple MS method, a final channel reduction step is cluster averaging, provided channel clusters exist, a cluster being defined as a group of four adjacent channels with all four weighting functions peaking at the same level. For each such cluster occurring in the set of selected channels, a single "cluster channel" is retained, which exhibits reduced measurement noise due to the averaging (for details see Lerner et al., 2002). Regarding Fig. 1, the clustering step slightly affected the final number of channels in Fig. 1a and 1c: 20 clusters were found in the case of Fig. 1a, reducing the 866 channels from the IC method to a final number of 806 channels, and 35 clusters in the case of Fig. 1c reducing the 860 channels from the MS method to a final number of 755 channels. No clusters could occur in the other cases (Fig. 1b and 1d) with only ≤ 2 channels per level.

Inter-comparison of the four cases shows that the spectral regions of selected channels are quite similar in all cases, i.e., the IC method and the MS method led to similar channel sets (the latter more efficiently, though). The < 100 channel cases (Fig. 1b and 1d) represent "high information content" subsets of the ~800 channel cases (Fig. 1a and 1c). The highest fraction of channels was selected from the water vapor absorption band between ~1150 and 1600 $cm^{-1}$. Further "source regions" are the 600–740 $cm^{-1}$ $CO_2$ band, a lower-troposphere $H_2O$ region near 2000 $cm^{-1}$, and the strongly absorbing $CO_2$ band near 2350 $cm^{-1}$, respectively. Only a few surface channels were selected, which is sufficient for the present upper air profiling purpose. Temperature retrieval results based on using the four different channel sets are discussed in Sect. 5.

## 4 Optimal estimation retrieval algorithm

Given a vector **y** of noisy brightness temperature values $T_B$ measured by the selected channels, an inverse model **I**(**y**) is required so that $\hat{\mathbf{x}} = \mathbf{I}(\mathbf{y})$ is an optimally estimated state $\hat{\mathbf{x}}$ (temperature profile **T**) retrieved from the measurements.

We utilized the iterative Gauss-Newton optimal estimation algorithm described in detail by Rodgers (2000). This algorithm is consistent with the adopted forward model (Eq. 2) and includes *a priori* information on the atmosphere in a transparent manner, the latter being required as the inversion of satellite radiometer data to atmospheric profiles belongs to the class of ill-posed inversion problems (e.g., Rodgers, 2000). The algorithm reads

$$\mathbf{x}_{i+1} = \mathbf{x}_a + \mathbf{S}_i \mathbf{K}_i^T \mathbf{S}_\varepsilon^{-1} [(\mathbf{y} - \mathbf{y}_i) - \mathbf{K}_i (\mathbf{x}_a - \mathbf{x}_i)], \quad (6)$$

where the subscript $i$ is the iteration index, $\mathbf{x}_{i+1}$ is the state vector iterated from the previous state $\mathbf{x}_i$ (retrieved temperature profile after $i$ iterations), $\mathbf{x}_a$ is an *a priori* state (temperature profile), $\mathbf{K}_i$ is the Jacobian defined in Sect. 2 evaluated at state $\mathbf{x}_i$, $\mathbf{y}_i$ are the measurements predicted by state $\mathbf{x}_i$, $\mathbf{S}_i$ is the retrieval error covariance matrix denoted $\hat{\mathbf{S}}$ in Eq. (4), and the other quantities involved ($\mathbf{y}$, $\mathbf{S}_\varepsilon$, $\mathbf{S}_a$) are as defined earlier. $\mathbf{K}_i$ and $\mathbf{y}_i$ have to be computed by the RTIASI forward model at each iteration step. Practically, Eq. (6) was iterated until the scalar cost function measure

$$\chi^2 = (\mathbf{y} - \mathbf{y}_i)^T \mathbf{S}_\varepsilon^{-1} (\mathbf{y} - \mathbf{y}_i) + (\mathbf{x}_i - \mathbf{x}_a)^T \mathbf{S}_a^{-1} (\mathbf{x}_i - \mathbf{x}_a) \quad (7)$$

fulfilled $\chi^2 < N_{ch}$, where $N_{ch}$ is the number of channels assembled in $\mathbf{y}$, approximately corresponding to the number of degrees of freedom involved (Rodgers, 2000). Furthermore, in the event this criterion was not met, the iteration was stopped when $\chi_i^2 > \chi_{i-1}^2$ (i.e., $\chi^2$ no longer decreasing) or, if also this 2nd criterion was not met, after a maximum number of 6 iterations. In order to aid convergence during the first one or two iterations, the so-called "D-rad" method (Liu et al., 2000) was applied as described by Lerner et al. (2002), with the control parameter "$\alpha$" set to 4 in this study. This aid is, in particular, helpful in case of poor *a priori* profiles. For the retrievals discussed in Sect. 5, typically 1–3 iterations were required until one of the above criteria ($\chi^2 < N_{ch}$ or $\chi_i^2 > \chi_{i-1}^2$) was properly met. As expected, slightly less iterations were in average needed for optimal retrieval cases compared to sub-optimal ones, where biased $\mathbf{x}_a$ profiles inconsistent with the $\mathbf{S}_a$ matrix were involved (Sect. 5). We denote the finally accepted best state estimate $\mathbf{x}_i$ by $\hat{\mathbf{x}}$ and its associated retrieval error covariance matrix estimate $\mathbf{S}_i$ by $\hat{\mathbf{S}}$. The final estimate $\mathbf{K}_i$ is simply termed $\mathbf{K}$.

Besides $\hat{\mathbf{S}}$, providing information on the retrieval error standard deviations and error correlation functions, and weighting matrix $\mathbf{K}$, quantifying the sensitivity of the measurements $\mathbf{y}$ to the state $\mathbf{x}$, some other quantities provide useful insight into properties of the profiles retrieved via Eq. (6). These include the gain matrix $\mathbf{G}$, the averaging kernel matrix $\mathbf{A}$, and the signal-to-noise ratio (SNR) matrix $\tilde{\mathbf{K}}$. All of these are described in detail by Rodgers (2000) so that they are only briefly explained here as needed for the discussion in Sect. 5. The gain matrix, defined as

$$\mathbf{G} = \partial\hat{\mathbf{x}}/\partial\mathbf{y} = \hat{\mathbf{S}}\mathbf{K}^T\mathbf{S}_\varepsilon^{-1}, \quad (8)$$

expresses the sensitivity of the estimated state $\hat{\mathbf{x}}$ to the measurements $\mathbf{y}$ and corresponds to the factor before the brackets in Eq. (6). The columns of **G**, the gain functions, also termed contribution functions, quantify how much a specific measurement $y_i$ contributes to $\hat{\mathbf{x}}$. The averaging kernel matrix reads

$$\mathbf{A} = \partial\hat{\mathbf{x}}/\partial\mathbf{x} = \mathbf{GK} \quad (9)$$

and expresses the sensitivity of the retrieved state $\hat{\mathbf{x}}$ to the "true" state **x**. The rows of **A**, the averaging kernel functions, also termed resolution kernels, generally peak at the diagonal of **A** and the width at half maximum of this peak is a measure of the spatial resolution of $\hat{\mathbf{x}}$ at the height level of the peak. The SNR matrix is defined as

$$\tilde{\mathbf{K}} = \mathbf{S}_\varepsilon^{-\frac{1}{2}} \cdot \mathbf{K} \cdot \mathbf{S}_a^{\frac{1}{2}}, \quad (10)$$

where the diagonal of $\tilde{\mathbf{K}}$ estimates the SNR profile associated with $\hat{\mathbf{x}}$ and its rows, the SNR functions, indicate the relative influence of measurement and *a priori* uncertainties at different height levels, respectively. More thoroughly exploited, the number of singular values of $\tilde{\mathbf{K}}$ greater than about unity expresses the effective number of independent measurements made to better than measurement noise level.

Finally, it is instructive to decompose the retrieval error covariance matrix $\hat{\mathbf{S}}$ into two components of the form

$$\hat{\mathbf{S}} = (\mathbf{A} - \mathbf{I}_n)\mathbf{S}_a(\mathbf{A} - \mathbf{I}_n)^T + \mathbf{G}\mathbf{S}_\varepsilon\mathbf{G}^T, \quad (11)$$

where $\mathbf{I}_n$ is the identity matrix. The first r.h.s. term is the so-called smoothing error covariance and the second one the measurement-based error covariance, respectively, the former expressing the contribution of the *a priori* errors to $\hat{\mathbf{S}}$, the latter the one of the measurement errors.

Regarding covariance specifications, a realistic non-diagonal $\mathbf{S}_\varepsilon$ matrix was adopted based on the best available current noise model for IASI brightness temperature data (P. Schluessel, EUMETSAT, Darmstadt, Germany, priv. communications, 2000) in the form detailed by Lerner et al. (2002). Typical instrumental noise values lie below 0.5 K and the off-diagonal elements of $\mathbf{S}_\varepsilon$ represent inter-channel correlation up to the third neighboring channel reflecting the apodization process involved in IASI spectra.

Forward model (RTIASI) deficiencies were accounted for in $\mathbf{S}_\varepsilon$ by adding for all channels 0.2 K to the instrumental errors (J. Eyre, The Met. Office, Bracknell, U.K., priv. communications, 2000). While this simplified treatment of forward modeling errors is reasonable in this initial study, an improved formulation more accurately reflecting RTIASI imperfections will be adopted in the future. The simulated noisy measurements **y** entering Eq. (6) were prepared to contain randomly generated noise consistent with this formulation of $\mathbf{S}_\varepsilon$ (without the forward model error component).

The *a priori* error covariance matrix $\mathbf{S}_a$ shall reflect the statistical uncertainty according to which the *a priori* temperature profile $\mathbf{x}_a$ typically deviates from the "true" profile **x** and was specified as follows. The square-roots of the diagonal elements of $\mathbf{S}_a$ (standard deviations) were set to 3 K at surface level (bottom) linearly increasing to 10 K at 0.1 mbar (top). This simple specification of error magnitudes was adopted after inspecting the *rms* error of an ensemble of about 100 difference profiles ($\mathbf{x}_a - \mathbf{x}$) relevant in our context (Sect. 5). It roughly reflects the uncertainties of climatological profiles relative to actual "weather" states of the atmosphere, though tending to be, for example, too optimistic at tropopause levels, where uncertainties can be quite higher (Sect. 5.3 addresses aspects of consistency between profiles $\mathbf{x}_a$ and covariance matrix $\mathbf{S}_a$). The non-diagonal elements of $\mathbf{S}_a$ were specified by using a correlation length $L$ = 6 km and imposing an exponential drop-off correlation according to $S_{ij} = \sigma_i \sigma_j \exp(|\, z_i - z_j \,| / L)$, where $\sigma_i = \sqrt{S_{ii}}$ is the standard deviation at height level $z_i$ and $\sigma_j$ the one at level $z_j$, respectively.

When requiring profile errors strictly consistent with a covariance matrix, the fact was exploited that any covariance matrix **S** can be decomposed into the form $\mathbf{S} = \sum_i \mathbf{e}_i \mathbf{e}_i$, where $\mathbf{e}_i = \lambda_i \mathbf{l}_i$ are the error patterns, i.e., the eigenvectors $\mathbf{l}_i$ of **S** scaled by the corresponding eigenvalues $\lambda_i$ (Rodgers, 2000). The error realization to be superposed on any individual profile **x** can then be expressed by

$$\boldsymbol{\varepsilon}_x = \sum_i a_i \mathbf{e}_i \,, \qquad (12)$$

where the scalar factors $a_i$ are normally distributed random deviates with unit variance (computed by any standard normal random numbers generator).

We utilized Eq. (12) in order to generate humidity profile realizations involving reasonable humidity uncertainties. Such profiles were required (together with ozone profiles, which are non-critical) as prescribed input profiles in the temperature-only retrieval process employed in this study. We assumed a humidity error covariance matrix $\mathbf{S}_q$ with constant diagonal element square-roots of 0.15 in ln(*specific humidity*) (up to the 200 mbar level above which humidity is negligibly small). This 15 % uncertainty roughly reflects the ~10–15 % uncertainty expected for humidity profiles if retrieved together with temperature profiles from IASI data (e.g., Collard, 1998; Lerner et al., 2002). The non-diagonal elements of $\mathbf{S}_q$ were computed assuming an exponential drop-off with a correlation length of 3 km. For generating the actual profile realizations the $\boldsymbol{\varepsilon}_x$ vectors obtained via Eq. (12) were simply added to the "true" humidity profiles. A further fully analogous use of Eq. (12) was made in Sect. 5.3 when checking the relevance of statistical consistency between $\mathbf{x}_a$ and $\mathbf{S}_a$.

## 5 Results and discussion

IASI measurements were simulated on the gridded latitude-height slice shown in Fig. 2 (top). We mainly discuss here temperature profile retrieval results in the latitude range 22°N to 45°N (Fig. 2, bottom), being a representative (subtropical) part of the slice. In the empirical error analysis of Sect. 5.3 a similar part of the southern hemisphere is used in addition (45°S to 22°S). The temperature slice was adopted, together with the corresponding humidity slice (not shown), to supply the "true" profiles **x**. The slices were extracted from the high-resolution (T213L50) weather analysis of the European Centre for Medium-range Weather Forecasts (ECMWF) of September 15, 1999, 12 UTC, at 79°W. The atmosphere was assumed to be sounded at latitude steps of 0.475°, which corresponds to the IASI scan-line separation of ~52.7 km and mimics the sub-satellite track of IASI IFOVs near nadir. 49 profiles were acquired over the 22°N to 45°N range in this way.

The climatological CIRA86aQ model (Kirchengast et al., 1999) was employed for supplying the *a priori* **T** profiles $\mathbf{x}_a$ at the locations and for the month of interest, which for this purpose just interpolates between **T** profiles of the original CIRA-86 tabular model (Fleming et al., 1988). The retrieval algorithm (Eq. 6) was initialized with $\mathbf{x}_0 = \mathbf{x}_a$. Humidity profiles where prescribed as discussed at the end of the previous section and a U.S. standard mid-latitude ozone profile was supplied to RTIASI as

reasonable ozone specification. In order to account for the latitudinally varying temperature structure in the channel selection, channel sets were pre-computed at every $10^{th}$ deg of latitude based on the CIRA86aQ September climatology. Channel sets have been prepared for all four cases illustrated in Fig. 1 based on either the IC or MS method as applicable (see Sect. 3). For the retrieval, always the channel set closest to the profile of interest was employed. With the MS method, it is even feasible to perform the channel selection for each individual sounding based on the available individual *a priori* profile. In this case the computation of the Jacobian **K** (in Eq. 5) required once per sounding for several thousand channels is the dominating efficiency-limiting factor.

### 5.1 Temperature field retrieval performance

Figure 3 depicts the **T** retrieval performance results for the **T** field in the latitude range 22°N to 45°N (49 profiles). "Retrieved-minus-true" **T** difference fields are shown for each of the four channel selection cases illustrated in Fig. 1a to 1d.

Considering the results of any of the four cases, tropospheric **T** profiles above ~800 mbar turn out to be retrieved with quite satisfactory quality (to better than 1 K in most places). Other areas, including the boundary layer, the equatorial tropopause region and parts of the stratosphere, show larger deviations from the "true" field (> 2 K over extended areas). The primary reason for these larger deviations lies in the magnitude and shape of the weighting functions, which exhibit largest values and best narrowness in the troposphere. On the other hand, only a few weighting functions have their peaks in the boundary layer and weighting functions (and the related resolution kernels) are too broad above 200 mbar to properly resolve the equatorial tropopause (cf. Sect. 5.2). In the stratosphere, also the increasing influence of the *a priori* profiles, not sufficiently unbiased, contributes to the systematic deviations over extended areas (cf. Sect. 5.3). As in the stratosphere the weighting functions are fairly weak and broad, the estimated state $\hat{\mathbf{x}}$ generally tends towards the *a priori* state $\mathbf{x}_a$ since not enough measurement information is contained in **K** about the "true" state.

Inter-comparing the results of the four different cases, the general picture is that the performance differences are not tremendous, though the algorithmic efficiency was of course significantly better for the < 100 channel cases (Fig. 3b and 3d). Inspecting more closely, the < 100 channel cases exhibit in fact slightly better performance, which is especially visible in the troposphere. This suggests that, for an estimation algorithm based on Eq. 6 and a forward model performance as involved here, the allowance for

more than ~1% of the total number of IASI channels does not improve the **T** retrieval (it rather becomes, besides less efficient, more sensitive to numerical errors with increasing dimensions of vectors and matrices). Results based on optimal retrieval for these four cases, where the $\mathbf{x}_a$ profiles are fully consistent with the $\mathbf{S}_a$ matrix, confirm this finding (see Sect. 5.3 below). Preliminary results for joint retrieval of temperature and humidity profiles indicate that about twice the number of channels (~2% of the total number) is sufficient in that case. For inspecting how the MS channel selection method (Sect. 3.2) performs relative to the IC method (Sect. 3.1) Fig. 3b and 3d need be examined. The major distinction may be found in the boundary layer in some areas, where the IC method does a slightly better job. Above the boundary layer, retrieval results are quite similar. This suggests that, since the MS method is significantly simpler to implement and more efficient, it is an attractive substitute for the IC method for many applications. In this study, all results discussed in the remainder have been produced based on < 100 channel sets selected by the MS method.

### 5.2 Temperature profile retrieval characteristics

In order to inspect the errors and various characteristics of retrieved **T** profiles in some detail, one typical vertical profile is extracted from Fig. 3d for closer investigation, namely the one at ~25°N latitude.

Figures 4a and 4b instructively confirm that temperatures near the tropopause and in some stratospheric regions are most difficult to retrieve. The large differences at the tropopause (~100 mbar) originate mainly from the limited resolution available above 200 mbar and from a too optimistic *a priori* error assumption (about 4.5 K at 100 mbar; see the definition of $\mathbf{S}_a$ in Sect. 4). Figure 4c illustrates the estimated retrieval error. The estimated total errors (i.e., the square roots of the diagonal elements of $\hat{\mathbf{S}}$) depend mainly on the shape of the weighting functions as well as on the assumed *a priori* errors (cf. Eq. 4). This total error estimate is, in turn, mostly determined by the smoothing error (square roots of the diagonal elements of the smoothing error covariance; Eq. 11), which is largest in the stratosphere where the *a priori* errors are important and the resolution kernels in **A** (discussed below) are broad. The measurement-based error (square roots of the diagonal elements of the measurement-based error covariance; Eq. 11) depends on the shape of **G** (discussed below) and is comparatively small as the instrumental errors specified in $\mathbf{S}_\varepsilon$ are small.

Figures 4d and 4e visualize the improvement furnished by the retrieval over the *a priori* knowledge in terms of showing the "error envelope" (dashed lines) about the mean profile (solid line) before (Fig. 4d) and after (Fig. 4e) the retrieval. The improvement due to the IASI measurements is most pronounced at tropospheric heights but still significant at stratospheric heights. The influence of the *a priori* data is well indicated in Fig. 4f by the "retrieval-to-*a priori*" error ratio profile (percentage ratio of estimated total retrieval errors to *a priori* errors). The 50 % line (dotted vertical) crossed near 200 mbar implies that the *a priori* data have a major influence in the stratosphere, while the measurements improve more than a factor of 2 upon the *a priori* errors in the troposphere.

Figure 5 illustrates further characteristics of the typical **T** profile including error correlation functions of $\mathbf{S}_a$ (a) and $\hat{\mathbf{S}}$ (b), weighting functions (c), averaging kernel functions (d), gain functions (e), and SNR functions (f). Correlation functions (rows of $\mathbf{S}_a$ and $\hat{\mathbf{S}}$; Eq. 4) and averaging kernel functions (rows of **A**; Eq. 9) are shown for clarity at three selected pressure levels only (~700, ~200, and ~10 mbar), representing the troposphere, tropopause region, and stratosphere, respectively. Correspondingly, weighting functions (rows of **K**), gain functions (columns of **G**; Eq. 8), and SNR functions (rows of $\tilde{\mathbf{K}}$; Eq. 10) are shown for three representative channels only, which exhibit peaks close to the three levels chosen. The diamond symbols indicate the retrieval levels (i.e., represent the actual values of the matrix elements) and are a reminder of the use of non-equidistant levels.

The correlation functions (rows of the normalized covariance matrix $C_{ij} = S_{ij} / \sqrt{S_{ii} S_{jj}}$) quantify the fraction of correlation between the error at a given level *i* with the one at any other level *j*. The correlations in $\mathbf{S}_a$ (Fig. 5a) follow the exponential drop-off structure as specified in Sect. 4. The retrieval errors obtained in $\hat{\mathbf{S}}$ show a somewhat akin but significantly sharpened correlation structure (Fig. 5b). This indicates that the errors in retrieved **T** profiles are largely uncorrelated (somewhat anti-correlated) between neighboring levels, the sharpening being introduced by the transformed-$\mathbf{S}_\varepsilon^{-1}$ term dominating $\mathbf{S}_a^{-1}$ in Eq. (4). Weak correlation (ideally no correlation) is a favorable property, for example, if the data are assimilated by optimal interpolation, since it simplifies the covariance matrix formulation. Figure 5c shows the characteristic shapes of the weighting functions, where each function indicates the weighting with which the

**T** profile contributes to the $T_B$ observation of a particular IASI channel. While $T_B$ observations sensitive to the troposphere (e.g., at 1994.25 $cm^{-1}$) stem from rather narrow well defined regions, the weighting functions increasingly broaden in the stratosphere, where their spread is of the order of 10 km (e.g., at 669 $cm^{-1}$). It is evident from this type of sensitivity (and the fact that more IASI channels peak in the troposphere than in the stratosphere) that the inversion will lead to retrievals with better accuracy and resolution in the troposphere than in the stratosphere.

Figure 5d displays averaging kernel functions, which measure with the spread of their main peak (full width at half maximum, FWHM) the resolution of the retrieved profile at the level of the peak (cf. Sect. 4). This FWHM measure indicates a resolution of better than 3 km in the troposphere decreasing to near 10 km at 10 mbar, which is consistent with preliminary results of Collard (1998). A detailed resolution analysis reported by Weisz (2001), involving also resolution measures alternative to FWHM (Backus-Gilbert spread, data density; see Rodgers, 2000), led to resolutions of 1 to 3 km throughout the troposphere gradually decreasing to about 15 km near the stratopause.

The gain functions (Fig. 5e) indicate that any specific observation contributes most to the retrieved profile near the peak of the associated weighting function. It may seem counter-intuitive, given the superior retrieval performance in the troposphere, that the largest gains (**T** units gained per unit $T_B$; cf. Eq. 8) occur for the stratospheric channel. Note, however, that the stronger gain function of the stratospheric channel does not only mean higher sensitivity of the retrieved state **T** to the measured $T_B$ but also correspondingly higher error amplification. Thus, other than weighting functions, gain functions do not directly indicate retrieval performance. SNR functions (Fig. 5f; computed for simplicity with diagonal $\mathbf{S}_\varepsilon$ and $\mathbf{S}_a$) resemble the shape of the weighting functions (Fig. 5c) as they are just normalized versions of them (Eq. 10). Their magnitude is governed in the troposphere mainly by the small measurement errors and in the stratosphere by the large *a priori* errors. The smaller peak value near 200 mbar is caused by the relatively large measurement errors (~0.8 K at 1558 $cm^{-1}$) of the "tropopause channels" near the center of the 1600 $cm^{-1}$ $H_2O$ band ($T_B$ < 240 K).

### 5.3 Empirical error analysis

We utilized *a priori* profiles $\mathbf{x}_a$ taken from a climatological model and specified the associated covariance matrix $\mathbf{S}_a$ in a relatively simplified way, as the actual error

statistics of the *a priori* profiles are difficult to capture. It warrants specific analysis how this type of simplification affected the quality of retrieval results. An empirical computation of relevant error measures (bias, standard deviation, standard error of bias, root-mean-square error) is performed for this purpose using the standard formulae for estimating these error measures given ensembles of "*a priori*-minus-true" or "retrieved-minus-true" difference profiles.

Figure 6 depicts the error profiles determined this way for both the ensemble of 49 profiles from the 22°N to 45°N range already used above (Fig. 6a–c) and an enlarged ensemble of 98 profiles comprising additional 49 profiles from the 45°S to 22°S range (Fig. 6d–f), respectively. The panels show the bias (*mean*; heavy solid), the doubled standard deviation of the bias (dotted; i.e., the *mean* lies with 95 % certainty within the dotted bounds), and the standard deviation (*stdev*; light solid) of an ensemble. In addition, the right-most panels (c and f) show the average of the theoretical retrieval error estimates obtained via $\hat{\mathbf{S}}$ (square-root of the diagonal; gray, heavy dashed) as well as the empirical *rms* retrieval error estimate ($rms^2 = bias^2 + stdev^2$; gray, heavy solid).

Figure 6a reveals a significant bias of the "*a priori*-minus-true" ensemble (the *a priori* profiles and "true" profiles were taken from the CIRA86aQ model and the ECMWF analysis field, respectively). This *a priori* bias leads to a significant bias of the "retrieved-minus-true" ensemble in the stratosphere (Fig. 6b), where the influence of *a priori* information is strongest (see, e.g., Fig. 4f). All errors are summarized in Fig. 6c, which highlights that in the troposphere the *rms* retrieval error equals the standard deviation since the bias is small, whereas above about 150 mbar the *rms* retrieval error is additionally determined by the bias. The theoretical retrieval error (gray dashed), while incidentally close to the empirical *rms* retrieval error (gray) in the troposphere, deviates in the stratosphere becoming increasingly overestimated. The discrepancy in the stratosphere stems from the biasedness of $\mathbf{x}_a$ and the over-simplification of $\mathbf{S}_a$ and thus from inconsistencies in the inversion process. Including the southern hemisphere profiles (Fig. 6d to 6f) confirms the features just discussed, though with somewhat different "*a priori*-minus-true" bias structure, which is the major cause of differences in detail between the 98 profile ensemble and the 49 profile ensemble. The main result is thus that the absence of consistency between *a priori* profiles and the associated covariance matrix can contribute appreciable retrieval errors in the stratosphere.

For verification purposes, we utilized *a priori* profiles $\mathbf{x}_a$ prepared via Eq. (12), which are consistent with the assumed $\mathbf{S}_a$ by construction and thus allow fully optimal retrievals. We tested these as alternatives to the climatological ones and performed the same empirical error analysis as illustrated in Fig. 6. Figure 7 depicts the results of this verification analysis. As confirmed by all panels, the bias is mostly gone and the overlap of the empirical *rms* retrieval error and the theoretically estimated retrieval error is rather close (Fig. 7c and f) except below 200 mbar. The larger values of the empirical error compared to the theoretical error in the troposphere originate from the 15 % uncertainty imposed upon the prescribed humidity profile realizations (Sect. 4); while the empirical estimate naturally accounts for it, the theoretical estimate $\hat{\mathbf{S}}$ essentially "overlooks" this humidity uncertainty in temperature-only retrievals (one could prevent this deviation by explicitly adding forward modeling errors to $\mathbf{S}_\varepsilon$, which account for the humidity uncertainty). Generally, Fig. 7 confirms that a consistent specification of *a priori* profiles and associated covariance matrix will render residual retrieval biases negligibly small also in the stratosphere.

We finally computed empirical and theoretical error estimates under optimal conditions (consistent $\mathbf{x}_a$ and $\mathbf{S}_a$) for all four channel set cases illustrated in Fig. 1 a–d, for the complete 98 profile ensemble. Figure 8 depicts the results, where Fig. 8d (the < 100 MS-selected channels case), is just a re-computation of the Fig. 7f case. Figure 8a–d confirms, for fully optimal retrievals, the main finding illustrated by Fig. 3a–d for sub-optimal retrievals, namely that using much more than ~1% of the IASI channels does not improve the temperature retrieval performance (cf. Fig. 8a,c with 8b,d). The smaller number of channels even seems to allow better retrieval close to the surface, but further study is needed to check the scope of validity of this specific result.

## 6 Summary and conclusions

Advanced high spectral resolution instruments like the Infrared Atmospheric Sounding Interferometer (IASI) furnish a very large number of channels (> 8000 channels in case of IASI). For a specific use of the data such as temperature profiling it is essential to reduce this number and to sensibly remove redundant information for purposes of computational efficiency and robustness of retrieval algorithms. In practical terms, measurement information from a given ensemble of channels can be considered redundant if removing that ensemble from the complete set of measurements produces

an insignificant decrease in retrieval accuracy or resolution (e.g., fractional change of retrieval error or resolution < 10%).

We introduced a simple and efficient channel selection method, termed “maximum sensitivity” method, the utility of which was investigated by one-to-one comparison with a more elaborate method directly following information content theory. Optimal estimation methodology was employed to solve the inverse problem of temperature retrieval. Based on optimal estimation retrieval, it was found that the temperature retrieval performance using the simple method is comparable to the one using the more elaborate method and, furthermore, that the number of IASI channels can be reduced to as low as ~1% of the total number of channels (i.e., to < 100 channels) without degrading the quality of retrieved temperature profiles (joint temperature and humidity retrieval needs about twice this number).

The retrieval algorithm was also used to investigate the effects of measurement errors and *a priori* uncertainties on temperature retrieval performance. A temperature field extracted from a high-resolution weather analysis of the European Centre for Medium Range Weather Forecasts (ECMWF) was used to supply “true” temperature profiles (as well as specific humidity profiles, which were perturbed with 15 % uncertainty in order to reflect the expected uncertainty of IASI specific humidity retrievals). For simulating IASI measurements and for computing Jacobian matrices the fast forward model RTIASI was used. The optimal estimation algorithm yielded temperature profiles, which significantly improved upon the *a priori* knowledge. Overall, a temperature accuracy of ~1 K was obtained at tropospheric heights (below ~200 mbar) associated with a resolution of 1 km (near surface) to 3 km (near tropopause). In the stratosphere the accuracy gradually decreased to ~3 to 4 K in the upper stratosphere (above ~10 mbar) with the resolution decreased to ~10 to 15 km.

Based on a representative subtropical profile, characteristic properties of retrieved temperature profiles were studied (correlation functions, weighting functions, resolution kernels, gain functions, signal-to-noise ratio functions). This provided quantitative insight into error structure and resolution as well as into the detailed role of both the measurements and the *a priori* information in furnishing the retrieval performance finally achieved. Tropospheric temperatures are fairly well sensed by the IASI instrument, *a priori* information almost becomes dispensable. Further into the stratosphere the retrieval is increasingly influenced by the *a priori* profiles. The retrieval performance strongly depends on magnitude and shape of the weighting

functions (e.g., clearly indicated by degraded performance in height regions associated with weak weighting functions such as the upper stratosphere).

The impact of (in)adequate modeling of *a priori* profiles and their covariance matrix has been assessed by an empirical error analysis. Using *a priori* profiles taken from a climatological model together with a covariance matrix only roughly reflecting the actual errors leads to a systematic "*a priori*-minus-true" bias, which is not accounted for by the optimal estimation inversion (practically, a bias correction would be required prior to the inversion). In this biased case, the empirical *rms* retrieval error estimate did not match the theoretical retrieval error estimate by the inverse algorithm in the stratosphere, where the *a priori* information exerts most influence. The stratospheric retrieval performance was improved by employing, for verification purposes, *a priori* errors generated by eigenvector decomposition of the *a priori* covariance matrix and thus consistent with the latter by construction. Residual stratospheric biases were found negligible in this verification case, which stresses the importance of consistent modeling of the *a priori* data and associated errors as well as the requirement that any ensemble of *a priori* profiles should be statistically unbiased against the corresponding ensemble of (in practice unknown) "true" profiles.

The results of the study confirm the potential of the IASI sensor for significantly improving upon atmospheric information available from current meteorological sounders and are encouraging for our continuation work on advancing the algorithm to joint temperature and humidity retrieval with emphasis on high-quality retrieval of upper tropospheric profiles (500 to 200 mbar domain). IASI-derived data of this type may become a future key database for the much needed monitoring of climatic changes in the thermal structure and moisture distribution of the troposphere.

*Acknowledgments.* We thank P. Schlüssel (EUMETSAT, Darmstadt, Germany) for helpful discussions on IASI characteristics as well as for providing the RTIASI model, which is a property of EUMETSAT, and the recent IASI level 1c noise model. Furthermore, we are grateful to M. Matricardi (ECMWF, Reading, U.K.) and J. Eyre (The Met. Office, Bracknell, U.K.) for valuable discussions on IASI performance and exchange of relevant recent results. The work of E.W. and J.A.L. was financially supported by the START research award of G.K. funded by the Austrian Ministry for Education, Science, and Culture and managed under Program No. Y103-CHE of the Austrian Science Fund.

(intentionally left blank; back page if double-sided print)

## References

Camy-Peyret, C., and Eyre, J. R., The IASI Science Plan, ISSWG (IASI Sounding Science Working Group) Report, ISSWG Office (P. Schluessel), EUMETSAT, Darmstadt, Germany (on-line via http://smsc.cnes.fr/IASI/), 1998.

Collard, A. D., Notes on IASI performance, Forecasting Research Techn. Report No. 256, 20p., The Meteorological Office, Bracknell, U.K., 1998.

Fleming, E. L., Chandra, S., Schoeberl, M. R., and Barnett, J. J., Monthly mean global climatology of temperature, wind, geopotential height and pressure for 0–120 km, NASA Techn. Memo. No. 100697, Nat. Aeron. and Space Admin., Washington, D.C., U.S.A., 1988.

Hanel, R. A., Conrath, B. J., Jennings, D. E., and Samuelson, R. E., Exploration of the Solar System by Infrared Remote Sensing, 458p., Cambridge Univ. Press, Cambridge-New York, 1992.

Lerner, J. A., Weisz, E., and Kirchengast, G., Temperature and humidity retrieval from simulated Infrared Atmospheric Sounding Interferometer (IASI) measurements, J. Geophys. Res., 107(D14), 4189, doi:10.1029/2001JD900254, 4-1–4-11, 2002.

Liu, X., Zaccheo, T. S., and Moncet, J-L., Comparison of different non-linear inversion methods for the retrieval of atmospheric profiles, Preprint Vol. of the 10$^{th}$ Conf. on Satellite Meteorology, Amer. Met. Soc. 2000 Annual Meeting, Long Beach, CA, U.S.A., 293–295, 2000.

Kirchengast, G., Hafner, J., and Poetzi, W., The CIRA86aQ_UoG model: An extension of the CIRA-86 monthly tables including humidity tables and a Fortran95 global moist air climatology model, Techn. Report for ESA/ESTEC No. 8/1999, 18p., Inst. for Geophysics, Astrophysics, and Meteorology, University of Graz, Austria, 1999.

Matricardi, M., and Saunders, R., A fast radiative transfer model for simulation of Infrared Atmospheric Sounding Interferometer radiances, J. Appl. Optics, 38, 5679–5691, 1999.

Rabier, F., Chafaï, D., and Abboubi, R., Comparison of channel selection methods for IASI, Proc. of the 11th International *A*TOVS Study Conf. (eds. J.F. LeMarshall and J.D. Jasper), Sept. 2000, Budapest, Hungary, 313–317, 2001.

Rodgers, C. D., Information content and optimisation of high spectral resolution measurements, Proc. of SPIE Conf. 2830 on Optical Spectroscopic Techniques and Instrumentation for Atmospheric and Space Research II (eds. P.B. Hays and J. Wang), 136–147, 1996.

Rodgers, C. D., Inverse Methods for Atmospheric Sounding: Theory and Practice, 256p., World Scientific Publ., Singapore, 2000.

Weisz, E., Temperature profiling by the Infrared Atmospheric Sounding Interferometer (IASI): Advanced retrieval algorithm and performance analysis (Ph.D. thesis), Wissenschaftl. Ber. No. 11, 174p., Inst. for Geophysics, Astrophysics, and Meteorology, University of Graz, Austria, 2001.

## Figures

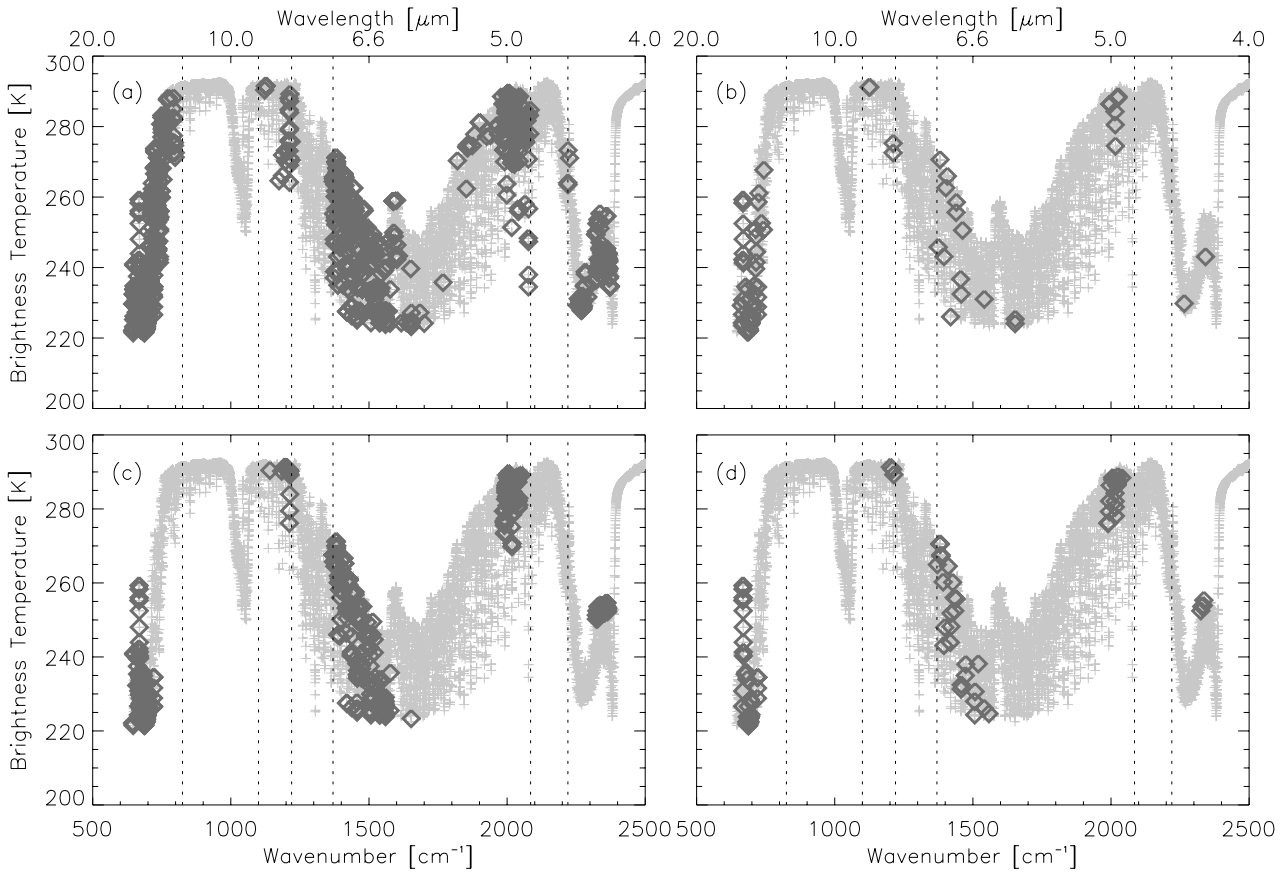


**Fig. 1.** Channel selection via (a) information content (IC) theory (final number 806 channels), (b) IC theory < 100 (72) channels, (c) "maximum sensitivity" (MS) method (final number 400 channels), and (d) MS method < 100 (86) channels. Selected-channel symbols (diamonds) are overplotted on the corresponding values of the brightness temperature spectrum (gray) computed for the U.S. standard mid-latitude summer atmosphere. Also indicated are "foreign" spectral bands (margins dotted) removed before IC or MS channel selection.

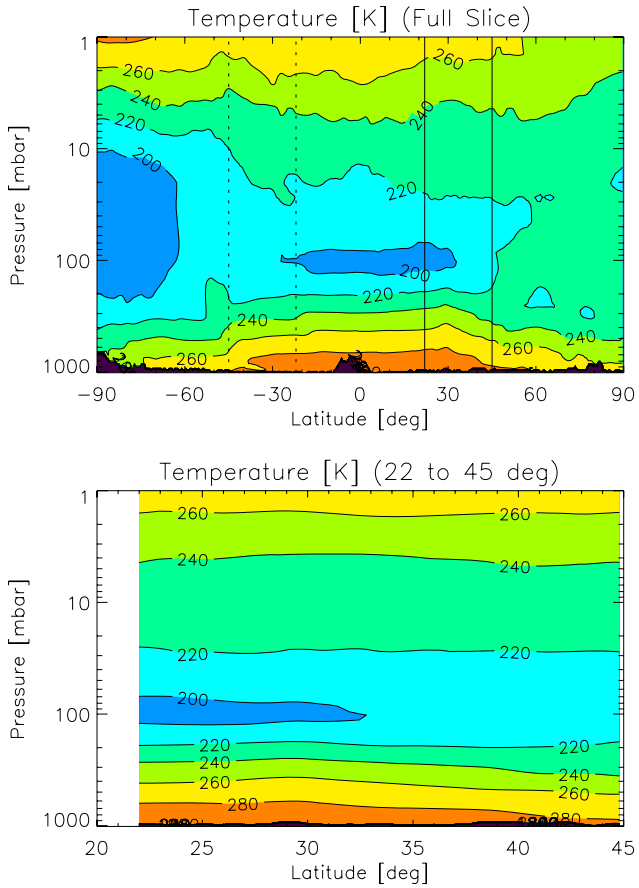


**Fig. 2.** "True" latitude-height temperature slices at longitude 79°W (ECMWF analysis, T213L50, Sept. 15, 1999, 12 UTC). Top: Pole-to-pole slice with 22°N to 45°N main subslice (margins solid) and 45°S to 22°S auxiliary subslice (margins dotted) indicated. Bottom: Enlarged view of the 22°N to 45°N subslice focused on in the study.

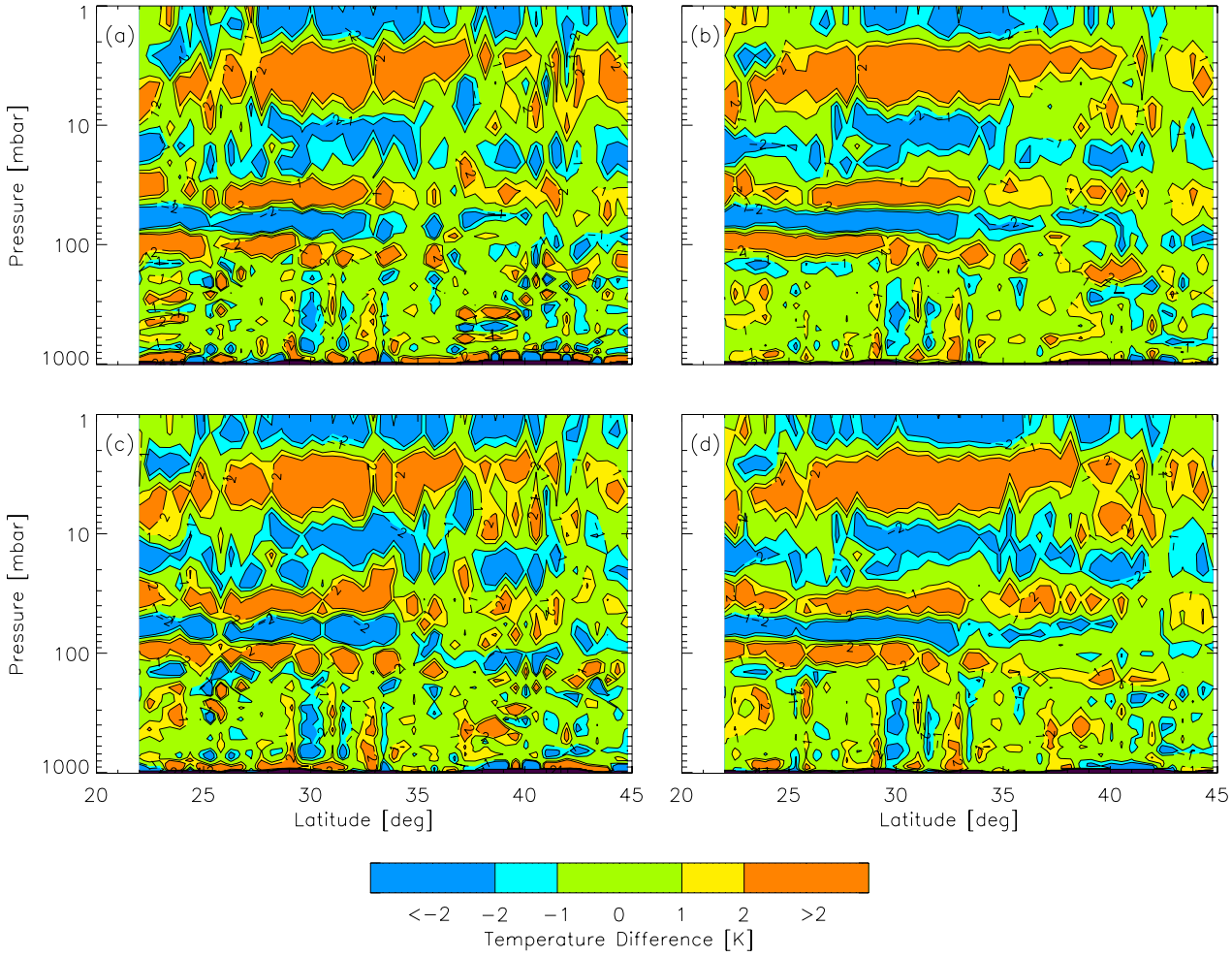


**Fig. 3.** Temperature difference fields ("retrieved-minus-true") for the 22°N to 45°N latitude range obtained when employing (a) 806 IC-selected channels, (b) 72 IC-selected channels, (c) 400 MS-selected channels, and (d) 86 MS-selected channels, respectively.

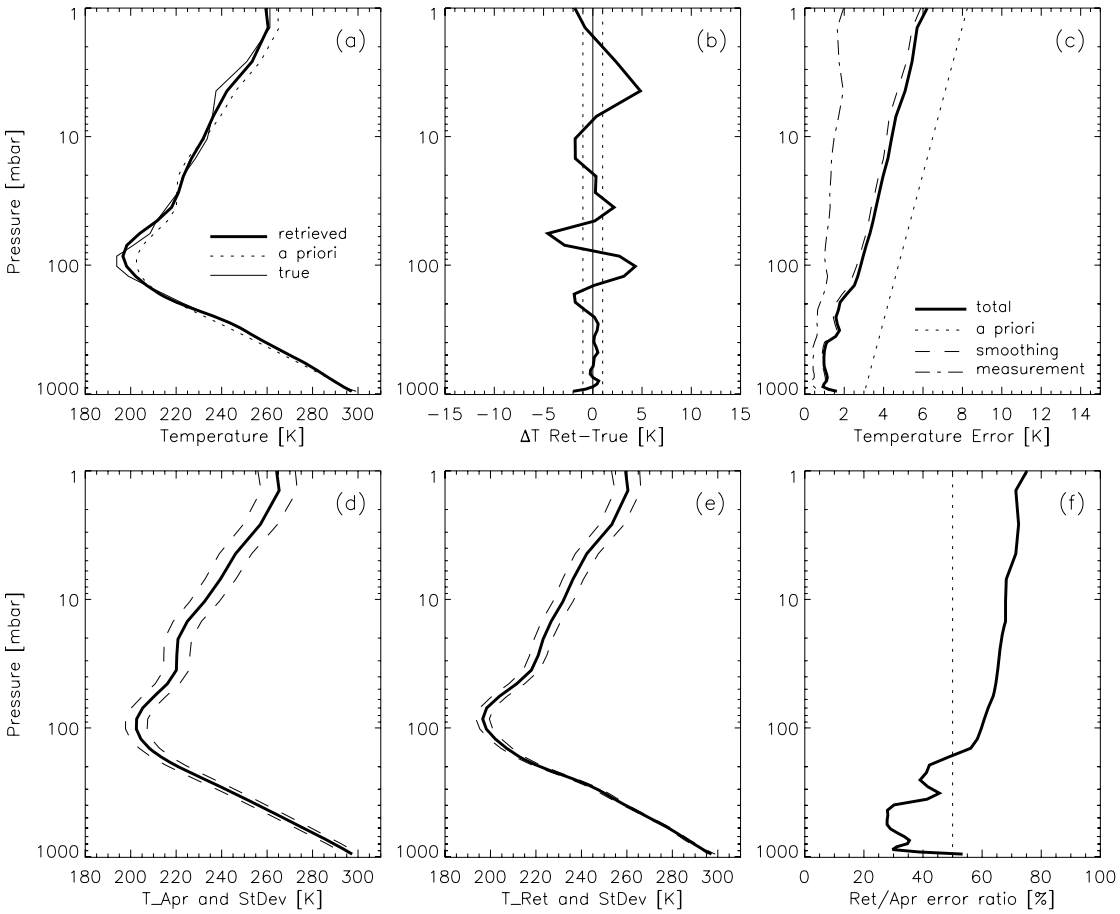


**Fig. 4.** Optimal estimation error analysis results for a typical temperature profile at latitude 24.85°N using 86 MS-selected channels. See Sect. 5.2 for explanation and discussion of panels a–f.

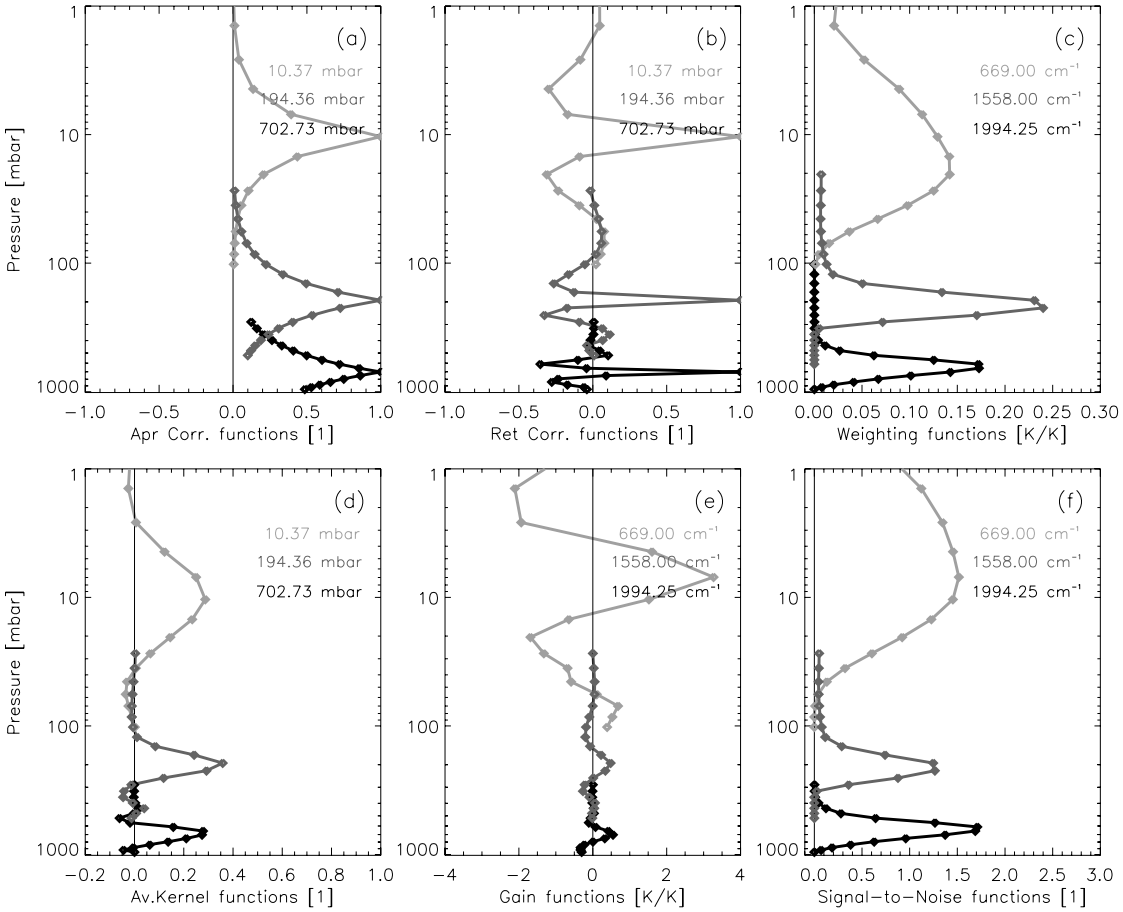


**Fig. 5.** Optimal estimation results for various functions characterizing retrieval performance for a typical temperature profile at latitude 24.85°N using 86 MS-selected channels. For clarity the functions are shown for three representative levels (~700, ~200, and ~10 mbar) and channels (1994.25, 1558.0, and 669.0 $cm^{-1}$) only. See Sect. 5.2 for explanation and discussion of panels a–f.

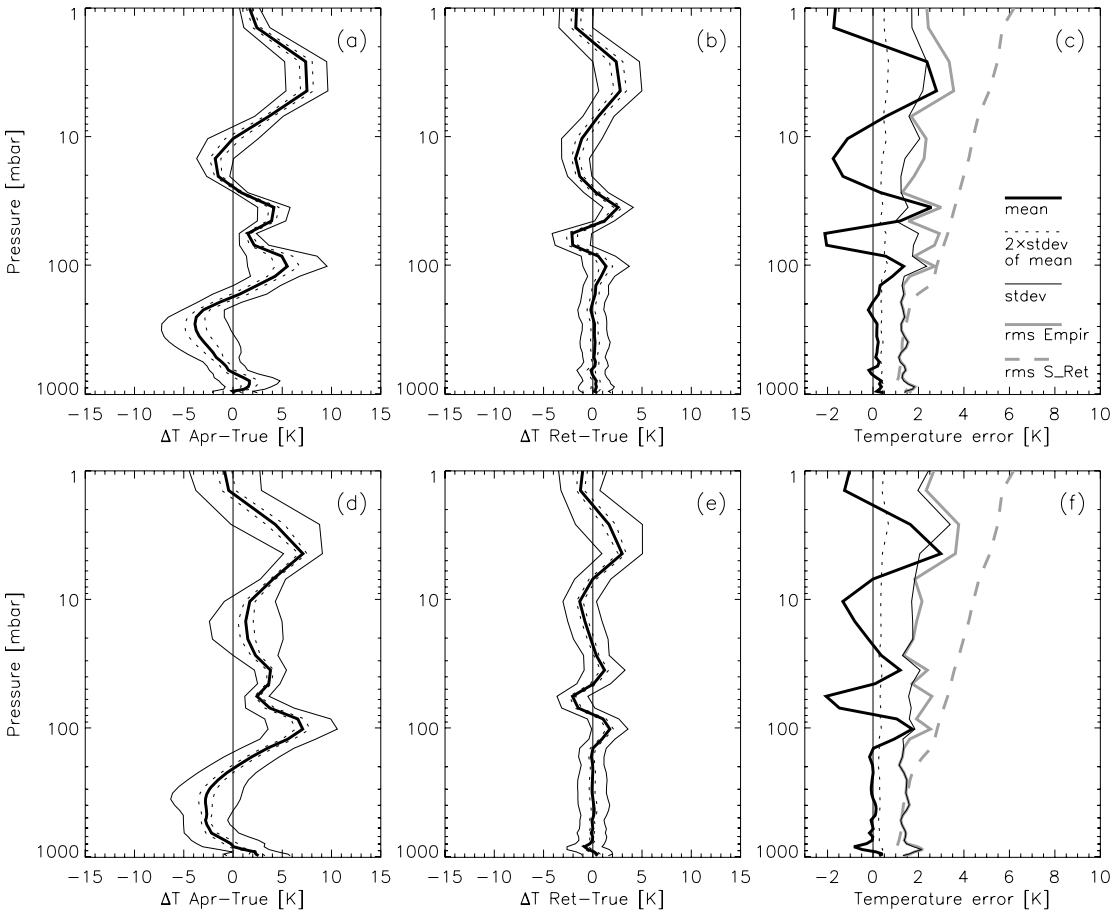


**Fig. 6.** Empirical error analysis results using the ensemble of 49 profiles from 22°N–45°N (top panels a–c) and of 98 profiles from 22°N–45°N plus 45°S–22°S (bottom panels d–f), respectively. The *a priori* profiles were taken from the CIRA86aQ climatological model. See Sect. 5.3 for explanation and discussion of panels a–f.

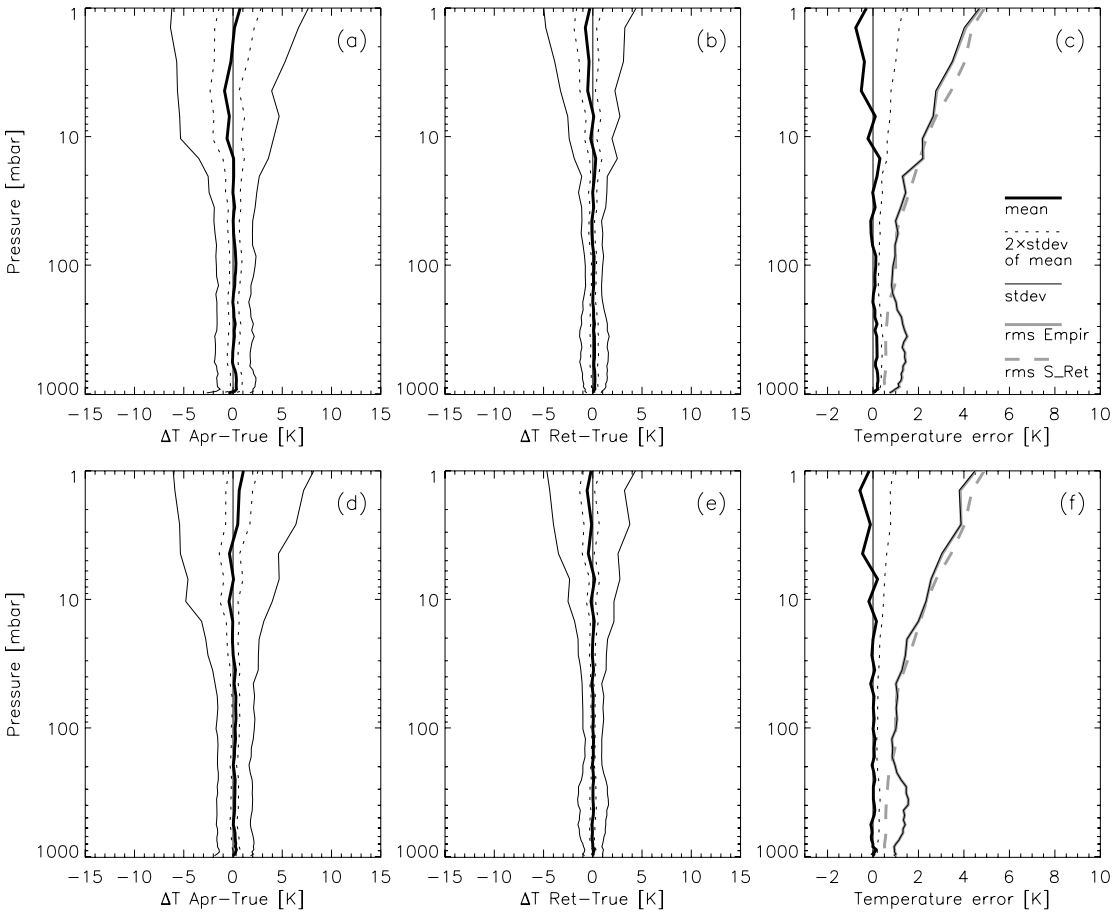


**Fig. 7.** Same as Fig. 6 except that *a priori* profiles exactly consistent with the *a priori* error covariance matrix were used.

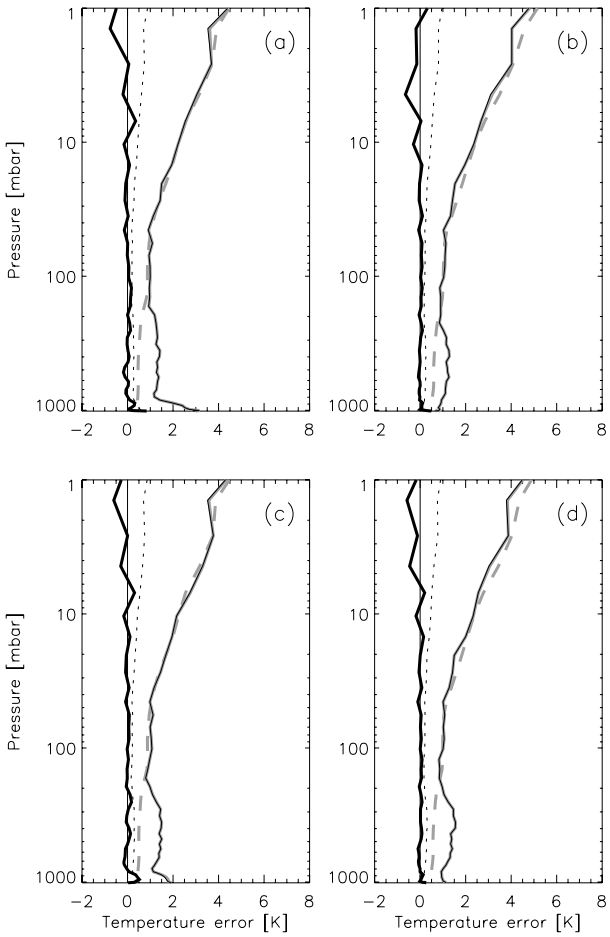


**Fig. 8.** Empirical error analysis results for the 98 profiles ensemble from 22°N–45°N plus 45°S–22°S using *a priori* profiles exactly consistent with the *a priori* error covariance matrix (same linestyles as in panels c and f of Fig. 6 and 7). The results were obtained for the same channel sets as used for Fig. 3: (a) 806 IC-selected channels, (b) 72 IC-selected channels, (c) 400 MS-selected channels, and (d) 86 MS-selected channels, respectively.

– end of document –